



# Influence of ns laser texturing of AISI 316L surfaces for reducing bacterial adhesion

Luca Romoli (2)<sup>a,\*</sup>, Gianmarco Lazzini<sup>a</sup>, Adrian H.A. Lutey<sup>a</sup>, Francesco Fuso<sup>b</sup>

<sup>a</sup> Department of Engineering and Architecture, University of Parma, 43124 Parma, Italy

<sup>b</sup> Dipartimento di Fisica Enrico Fermi, Università di Pisa, 56127 Pisa, Italy

## ARTICLE INFO

Article history:  
Available online 17 May 2020

Keywords:  
Laser  
Texture  
Antibacterial

## ABSTRACT

Nanosecond pulsed laser texturing has been performed on stainless steel with the objective of developing surface treatments to reduce bacterial adhesion on mechanical components in food handling machinery. The adhesion of *Escherichia coli* (*E. coli*) on four distinct textures has been investigated with standardised protocols for measurement of antibacterial performance. Surface morphology has been studied in detail for each texture to ascertain the presence of hierarchical structures and determine the role of topography in reducing bacterial adhesion. Despite the absence of sub-micrometric features comparable with bacterial size, this work highlights the crucial role that nanosecond pulsed laser irradiation plays in promoting a thin layer of iron oxide that reduces *E. coli* adhesion through local repulsive electrostatic interactions.

© 2020 CIRP. Published by Elsevier Ltd. All rights reserved.

## 1. Introduction

The growing interest in manufacturing textured smart surfaces mimicking the functional properties of natural interfaces has pushed scientists towards finding new, effective and easy-to-implement approaches for processing large areas. As a result, several techniques including electro-physical processes, and chemical and thermal treatments have seen significant research activity in relation to both the functionalities of processed surfaces as well as their adaptability to the requirements of industrial production [1]. Amongst these, laser texturing is particularly well-suited as it can be implemented within an industrial context for processing large areas on complex shapes [2]. Ultrashort pulsed lasers prevent target melting during laser-matter interaction, allowing the production of textures comprising sub-micrometric features with hierarchical regularity [3]. Such textures exhibit topographies very similar to biological interfaces having specific functionalities such as the self-cleaning lotus leaf or antimicrobial shark skin. In particular, the latter has inspired the idea of designing surface topography to influence surface bacterial adhesion and thus produce long-lasting and chemical-free antibacterial surfaces for the agrifood industry and/or in biomedical devices [4].

The working principle of such textured antibacterial surfaces is a complex interplay between surface morphology and chemistry; mechanisms that are still not fully understood. A large reduction in contact area between a bacterial cell and substrate creates an unsuitable environment for cellular attachment. Due to the small size of single bacterial cells ( $\sim 1 \mu\text{m}$ ), sub-micrometric protrusions induced by ultrashort laser pulses appear to be effective at producing antibacterial behaviour [5,6]. Despite the potential of ultrashort laser sources, their high setup cost

and relatively long processing times still make them difficult to implement in an industrial context. Conversely, despite their lower effectiveness in producing sub-micrometric structures, nanosecond lasers could represent a low-cost and more conventional alternative. Furthermore, nanosecond lasers offer the possibility of obtaining greater benefits in terms of surface chemistry. Nanosecond laser irradiation leads to the transfer of a small quantity of thermal energy to the target surface that produces an oxide layer on stainless steel in air with thickness ranging from tens to hundreds of nanometres [7]. These chemical compounds have been found to interfere with bacterial activity as their intrinsic anionic nature hinders bacterial adhesion [8].

Based on this hypothesis, the present work focuses on demonstrating the effectiveness of conventional nanosecond laser texturing in preventing contamination of AISI 316L stainless steel surfaces by *Escherichia coli* (*E. coli*), a common bacterial strain of significant importance within the agrifood industry. The main idea behind this approach is to create changes in surface morphology and chemistry by exploiting laser-induced material removal and oxidation of the target surface. The final objective is to demonstrate that surface textures characterised by sub-micrometric features are not always necessary to significantly reduce the formation of biofilm. Though nanosecond laser pulses are less effective at obtaining hierarchical surface structures, the production of a thin iron oxide layer may play a key role in lowering the adhesion of *E. coli* through chemical and electrostatic phenomena. Being biocompatible, such a solution could be widely used not only within the agrifood industry but also in biomedical science and pharmaceuticals.

## 2. Surface properties affecting bacterial adhesion

Experimental investigations have revealed that the sequence of events leading to the formation of biofilm depends on several surface

\* Corresponding author.

E-mail address: [luca.romoli@unipr.it](mailto:luca.romoli@unipr.it) (L. Romoli).

and environmental properties [9], including morphology, charge, chemistry, wettability and fluid dynamics. The boundary properties of a surface are always the result of interplay between surface topography and chemistry.

Biofilm formation involves several length scales ranging from the bacterial cell size during the initial stages of attachment to length scales compatible with wettability measurements during final stages. However, since attachment during the initial stage is expected to be a precursor of subsequent stages, bacterial size should represent one of the most relevant length scales of the entire sequence leading to a mature biofilm.

Several works have focused on finding a direct correlation between wettability and bacterial adhesion, leading to contrasting opinions [10]. In particular, Gupta et al. [11] mainly attribute the antibacterial behaviour of stainless steel substrates processed with nanosecond laser pulses to a decrease in surface wettability. However, measurement of this surface property with the standard sessile drop method is the result of the mean topography and chemical properties over a relatively large area that is not representative of initial bacterial interaction with the surface in a submerged environment.

Bacteria can be treated as colloidal particles due to their size, which ranges from hundreds of nm to a few  $\mu\text{m}$ . The ability of bacteria in a liquid solution to adhere to flat substrates can therefore be studied in terms of traditional theories relating to colloidal stability, such as the Derjaguin Landau Verwey Overbeek (DLVO) theory, describing the aggregation of aqueous dispersions [12]. The DLVO theory interprets interactions between a colloidal particle and a flat surface as the combination of attractive Lifshitz-Van der Waals and repulsive electrostatic interactions. The repulsive contribution that will be considered within this study is typically quantified in terms of the so-called Zeta potential [13]. This potential accounts for excess charge on a bacterial surface due to ionic exchanges with the surrounding liquid environment. Large absolute values of the Zeta potential are representative of strong surface repulsions. Conversely, small absolute values indicate attractive behaviour. The Zeta potential is a function of the pH of the solution in contact with the surface. In particular, by increasing the solution pH, the Zeta potential decreases, passing from positive to negative values as shown in Fig. 1.

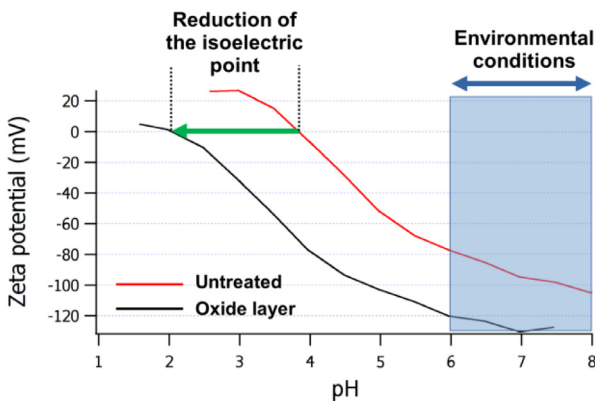


Fig. 1. Representative graph of the working principle of ns laser treated stainless steel surfaces [13,14]. Bacterial repulsion is induced by promoting a layer of oxides which lowers the Zeta potential within the pH range 6–8, environmental conditions compatible with bacterial life (in blue).

The so-called isoelectric point is a characteristic quantity representing the pH at which the Zeta potential changes sign. In relation to stainless steel, the Zeta potential has been widely studied [14], leading to an accepted value of the isoelectric point at  $\text{pH} \sim 4$ . Pulsed laser irradiation and oxide growth modify the composition of stainless steel substrates by reducing Cr concentration within the melt zone [7], leading to an abundance of surface iron oxides with a consequent reduction in the isoelectric point to  $\text{pH} \sim 2$  [13]. This reduction implies a global reduction of the Zeta potential for the treated stainless steel surface, as represented in Fig. 1. In particular, within the pH

range 6–8, representing environmental conditions compatible with bacterial life, high negative values of the Zeta potential may result in strong repulsion of bacterial cells which, with few exceptions, are characterized by a negative net charge [15]. The limited thermal effects promoted by nanosecond laser irradiation can therefore be exploited to induce controlled surface oxidation, which is expected to promote antibacterial behaviour.

### 3. Materials and methods

An Ytterbium-doped fibre laser with emission wavelength of 1064 nm and pulse duration of 104 ns was used to texture  $50 \times 50$  mm AISI 316L stainless steel specimens with an initial average areal surface roughness ( $S_a$ ) of 100 nm. A galvanometric scanning head with 160 mm focal length f-theta lens was used to scan the focused laser beam over the surface of each sample in a series of parallel lines while varying the velocity, hatch spacing and laser pulse fluence. All tests were performed in ambient air with a focused laser spot diameter of  $60 \mu\text{m}$ .

Four parameter groups, summarised in Table 1, were selected to determine the influence of the macroscopic surface topography and oxide layer thickness on antibacterial performance. Two laser scanning strategies were employed, the first comprising separate ablation craters with no pulse overlap (groups 1 and 2) and the second comprising linear grooves with 50% pulse overlap in the scanning direction and no overlap in the hatch direction (groups 3 and 4). Both strategies are shown schematically in Fig. 2, where typical characteristics of nanosecond laser-textured surfaces are highlighted, including the ablated volume, melt layer and oxide layer. These configurations were performed at moderate ( $24.8 \text{ J/cm}^2$ ) and high ( $60.1 \text{ J/cm}^2$ ) pulse fluence to vary the feature size and oxide layer thickness resulting from interaction between the laser beam and surface. Additional tests were performed with the same scanning strategies and pulse fluence over the range  $3.5\text{--}60.1 \text{ J/cm}^2$  to determine the maximum removal depth.

Table 1  
Laser parameters used for experiments.

| Parameter group                         | 1    | 2    | 3    | 4    |
|---|------|------|------|------|
| Average power (W)                       | 7    | 17   | 7    | 17   |
| Repetition rate (kHz)                   | 20   | 20   | 20   | 20   |
| Pulse energy ( $\mu\text{J}$ )          | 350  | 850  | 350  | 850  |
| Peak pulse fluence ( $\text{J/cm}^2$ )  | 24.8 | 60.1 | 24.8 | 60.1 |
| Scanning velocity (mm/s)                | 2000 | 2000 | 600  | 600  |
| Hatch spacing ( $\mu\text{m}$ )         | 100  | 100  | 100  | 100  |
| Average energy dose ( $\text{J/cm}^2$ ) | 3.5  | 8.5  | 11.7 | 28.3 |

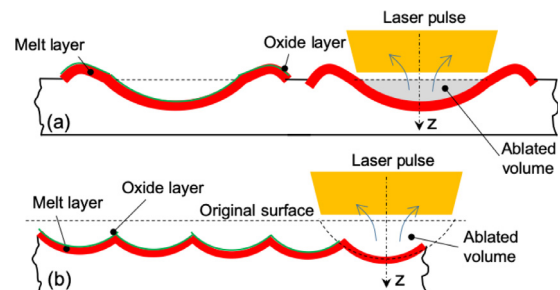


Fig. 2. Schematic representation of nanosecond pulsed laser irradiation with (a) separate ablation craters and (b) 50% pulse overlap in the longitudinal direction.

It was necessary to avoid ablation features with depths exceeding  $10 \mu\text{m}$  and high aspect ratios, as these represent favourable conditions for bacterial nesting at the bottom of valleys [6]. For this reason, the expected topography after laser exposure was calculated by considering the single pulse ablation depth as a logarithmic function of pulse fluence:

$$d_a = C_a \cdot \ln\left(\frac{F}{F_{th}}\right), F \geq F_{th} \quad (1)$$

where  $C_a = 1.25 \mu\text{m}$  and  $F_{th} = 3 \text{ J/cm}^2$  were determined through preliminary tests. The resulting surface topography following a single laser pulse was then calculated based on a Gaussian laser fluence distribution:

$$F = F_0 \exp\left(-2 \frac{x^2 + y^2}{w_0^2}\right) \quad (2)$$

where  $F_0$  is the peak pulse fluence and  $w_0$  is the focused laser spot radius ( $30 \mu\text{m}$ ). The topography was then determined by summing  $d_a$  for all laser pulses with longitudinal and lateral pulse separation distances corresponding to the scanning strategy.

The thickness of the surface oxide layer that forms after resolidification of the melt layer exhibits approximately linear dependence on the total energy dose where the pulse overlap is  $\leq 90\%$ , ranging from a few nanometres at low energy dose to 300–500 nm for doses in the order of  $400 \text{ J/cm}^2$  [7,16]. The oxide layer in the present study was therefore expected to be discontinuous for group 1 with a thickness of a few nm and uniform for the other groups with a thickness of 15–30 nm.

Microscopy was performed on the textured surfaces with an optical microscope equipped with 5–100 $\times$  objectives. A Taylor Hobson CCI-MP coherence scanning interferometer with 50 $\times$  objective (NA = 0.55) was employed for optical profilometry, achieving a resolution of  $<0.6 \mu\text{m}$  in the horizontal plane and  $<1 \text{ nm}$  in the vertical direction over a  $346 \times 346 \mu\text{m}$  sampling area. The cited resolutions were established in line with the requirements of ISO 25178-600 for geometric product specifications. Each surface profile obtained with the optical profiler was levelled, after which a very limited number of unmeasured points resulting from an insufficient or saturated signal were filled via interpolation. The average areal surface roughness was determined based on three samples for each texture type. Scanning shear-force microscopy (ShFM) was performed with a custom setup comprising a tungsten wire probe with 50 nm tip diameter attached to a quartz tuning fork that was maintained in dithering oscillation parallel to the sample surface. Damping of the oscillation in close vicinity to the surface (a few nm) was exploited in a closed-loop configuration to adjust the tip-sample distance and acquire the topography with a resolution of 1 nm in the horizontal plane and 0.1 nm in the vertical direction. Such a resolution enabled verification of the presence of nanoscale surface features possibly affecting bacterial attachment. ShFM maps were filtered to remove a very limited number of local defects parallel to the fast scanning direction.

Bacterial adhesion tests were performed with *E. coli* (ATCC 8739) based on ISO 22196 and ISO 27447 standards for measuring antibacterial performance. Bacterial colonies were transferred to Nutrient Agar (NA) and incubated for 24 h at 37 °C before being transferred again to NA and incubated at the same temperature for another 18 h to ensure that cells were free from environmental stress and in an appropriate growth phase. The stock was then diluted to N/500 and an optical density of 0.5 before being transferred into sterile containers where individual samples were immersed for two hours at 24 °C. During this test period, textured surfaces were held horizontally facing upwards while the containers were agitated at a frequency of 1.5 Hz and a stroke of 30 mm. Samples were then removed from the containers and held horizontally to remove excess fluid, before orthogonal surface swabs were taken over the entire surface area, diluted in solution, seeded in NA and incubated at 37 °C for 48 h. A colony counter was used to quantify the number of colony forming units per swab. Three identical samples were tested for each parameter group, together with three untextured control samples.

#### 4. Results and discussion

The measured surface topography of all laser-textured surfaces as acquired with the coherence scanning interferometer and ShFM is presented in Fig. 3. The measured average areal surface roughness

( $S_a$ ) based on three samples for each texture type was  $0.52 \mu\text{m}$ ,  $1.27 \mu\text{m}$ ,  $0.96 \mu\text{m}$  and  $1.84 \mu\text{m}$  for surfaces produced with parameter groups 1–4, respectively. The obtained values of  $S_a$  exhibited a dispersion of no more than  $0.05 \mu\text{m}$  between measurements. In the case of separate ablation craters obtained at moderate fluence (group 1), the limited diameter of craters led to incomplete surface coverage and a relatively low average areal surface roughness. The individual craters were nonetheless characterised by material removal in the central region and a circular ridge formed by movement of the liquid phase during laser exposure (see Fig. 2). With high pulse fluence (group 2), homogeneous surface coverage was achieved with a series of ablation craters whose ridges were predominantly in contact with those of surrounding craters. The scanning strategy with overlapping pulses led to a series of parallel grooves with maximum removal depth ranging from  $3.7 \mu\text{m}$  at  $24.8 \text{ J/cm}^2$  to  $6.2 \mu\text{m}$  at  $60.1 \text{ J/cm}^2$  and a corresponding increase in the average areal surface roughness. ShFM measurements excluded the presence of significant nanoscale features resulting from redeposition of ejected nano-particles during laser irradiation.

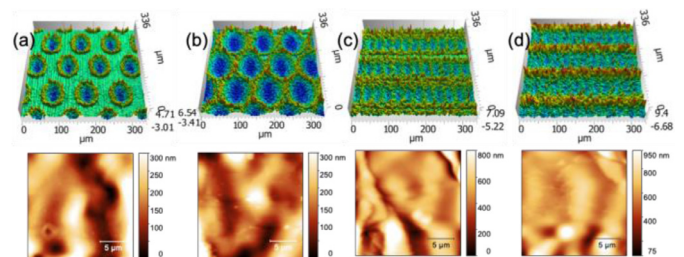


Fig. 3. Measured surface topography of parameter groups (a) 1, (b) 2, (c) 3 and (d) 4 with optical profiler (top) and ShFM in central region of crater/groove (bottom). ShFM scale bars represent  $5 \mu\text{m}$ .

The calculated and measured maximum removal depth is presented as a function of pulse fluence for both separate (groups 1 and 2) and overlapping (groups 3 and 4) laser pulses in Fig. 4. It can be observed that pulse overlap did not translate into greater removal depth until pulse fluence was sufficiently high to produce craters similar in size to the focused laser spot. As a result, the maximum ablation depth was identical with both scanning strategies up to  $8 \text{ J/cm}^2$ , after which higher removal depth was achieved at 600 mm/s than at 2000 mm/s. A minimum pulse fluence of  $24.8 \text{ J/cm}^2$  was therefore chosen for bacterial adhesion tests to ensure that grooves were achieved at 600 mm/s. The four test conditions employed for bacterial adhesion tests are indicated in Fig. 4.

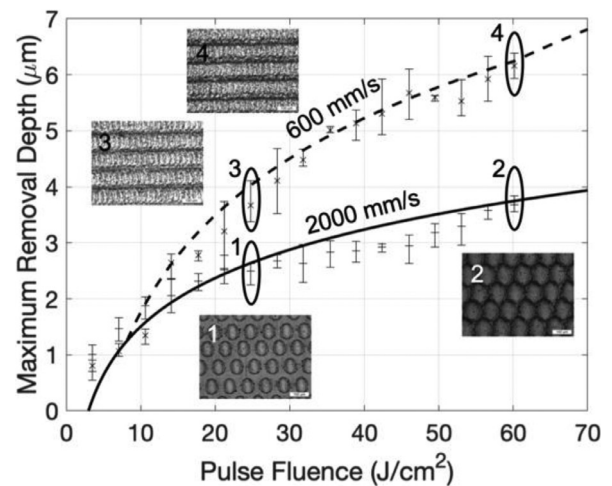


Fig. 4. Predicted (solid line: 2000 mm/s, dashed line: 600 mm/s) and experimental (+: 2000 mm/s, x: 600 mm/s) maximum removal depths as functions of laser pulse fluence, together with representative microscope images. Points 1–4 represent parameter groups given in Table 1. White microscope scale bars represent  $100 \mu\text{m}$ .

In terms of the expected effect of surface topography on bacterial adhesion, the macroscopic features present on all treated surfaces were generally too large and shallow to significantly reduce the contact area between the surface and bacterial cells of size  $\sim 1 \mu\text{m}$ . The lack of nanoscale features observed with ShFM suggests that uniform coverage of the surface with sub-micrometric protrusions such as those held responsible for antibacterial behaviour following ultrashort laser pulses were not present after nanosecond laser irradiation.

Fig. 5 presents the geometric average of the *E. coli* bacteria count after two hours of exposure to the bacterial solution. Values are normalised against the untreated control samples. An interpretation of the overall trend can be given by referring to the laser energy dose (Table 1). Highest bacterial adhesion was observed for samples treated with parameter group 1, corresponding to the lowest energy dose. Incomplete surface irradiation in this case implied the existence of regions between craters that were not oxidised. Thus, bacterial adhesion was expected to be similar to that of the control samples. Samples obtained with parameter groups 2 and 3 showed that by increasing the energy dose, the resulting treatment has strong antibacterial behaviour ( $\sim 98\%$  reduction). A further increase in energy dose (group 4) led to a rise in bacterial adhesion.

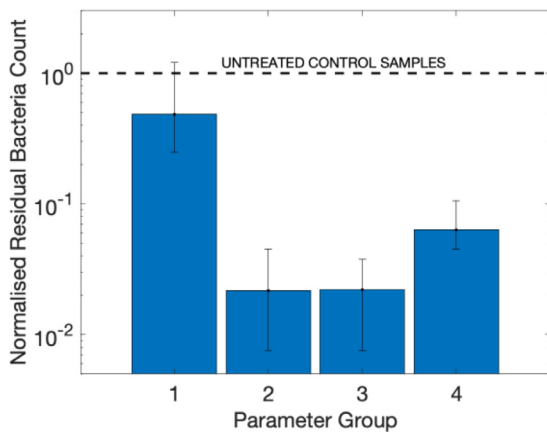


Fig. 5. Normalised residual *E. coli* count for surfaces treated with the parameter sets given in Table 1.

The large reduction in bacterial adhesion observed for parameter sets 2 and 3 can be interpreted in terms of the physical and chemical mechanisms involved in bacterial biofilm formation. Though it has been suggested in other studies [11] that surface topography plays a role in achieving antibacterial properties following nanosecond pulsed laser texturing, the resulting surface topography does not have the sub-micrometric features necessary to reduce the contact area between a bacterial cell of size  $\sim 1 \mu\text{m}$  and the surface. It is therefore expected that for samples 2 and 3 bacterial adhesion was mainly influenced by surface chemistry, in particular by the enhancement of electrostatic repulsions induced by a thin oxide layer promoted by laser treatment.

This reasoning, based primarily on the chemical contribution, can be considered valid in quasi-static conditions where cellular motion is deemed to be Brownian. If hydrodynamic forces are present, it can be expected that other effects could occur in the presence of large micrometric protrusions, such as protection against hydrodynamic turbulence. This could be an interpretation of the less pronounced reduction in bacteria count for sample 4, processed with highest energy dose and exhibiting a higher removal depth compared to samples 2 and 3. In the conditions employed during the contamination phase, in which the samples were continuously agitated, such a “sheltering effect” may have come into play. The sheltering effect

was expected to be less pronounced for samples 2 and 3, for which local effects relating to surface chemistry were expected to dominate, leading to improved antibacterial performance. Ideal process parameters were therefore those that led to complete coverage of the target surface but limited material removal.

## 5. Conclusion

Nanosecond pulsed laser irradiation has been found to be an effective approach for reducing *E. coli* adhesion on 316L stainless steel surfaces where the laser scanning strategy and pulse fluence are chosen to achieve homogeneous coverage of the surface with ablation features of limited depth ( $\leq 4 \mu\text{m}$ ). The mechanisms behind this antibacterial behaviour are fundamentally different to those taking place following ultrashort pulsed laser irradiation, where sub-micrometric protrusions reduce the contact area between bacterial cells and the substrate during the initial phases of attachment. For nanosecond laser pulses, this pathway is excluded due to the lack of significant nanoscale features. Chemical phenomena due to the formation of a thin iron oxide layer are instead more likely, as the presence of this phase leads to high negative values of the Zeta potential that result in strong repulsion of negatively charged particles such as bacteria. Results obtained with highest energy dose nonetheless imply that ablation features with high removal depth lead to protection of bacterial cells against hydrodynamic turbulence and are therefore less effective. Though it is clear that further investigation is required to verify the exact mechanisms with which bacterial adhesion is reduced, the possibility of utilising nanosecond laser pulses offers the prospect of lower cost laser-textured antibacterial surfaces in the near future.

## References

- [1] Malshe A, Bapat S, Rajurkar KP, Haitjema H (2018) Bio-Inspired Textures for Functional Applications. *CIRP Annals* 67(2):627–650.
- [2] Chun DM, Ngo CV, Lee KM (2016) Fast Fabrication of Superhydrophobic Metallic Surface Using Nanosecond Laser Texturing and Low-Temperature Annealing. *CIRP Annals* 65(1):519–522.
- [3] Römer GRBE, Huis in't Veld AJ, Meijer J, Groenendijk MNW (2009) On the Formation of Laser Induced Self-Organizing Nanostructures. *CIRP Annals* 58(1):201–204.
- [4] Fadeeva E, Truong VK, Stiesch M, Chichkov BN, Crawford RJ, Wang J, Ivanova EP (2011) Bacterial Retention on Superhydrophobic Titanium Surfaces Fabricated by Femtosecond Laser Ablation. *Langmuir* 27(6):3012–3019.
- [5] Epperlein N, Menzel F, Schwibbert K, Koter R, Bonse J, Sameith J, Krüger J, Toepel J (2017) Influence of Femtosecond Laser Produced Nanostructures on Biofilm Growth on Steel. *Applied Surface Science* 418:420–424.
- [6] Lutey AHA, Gemini L, Romoli L, Lazzini G, Fuso F, Faucon M, Kling R (2018) Towards Laser-Textured Antibacterial Surfaces. *Scientific Reports* 8(1):10112.
- [7] Adams DP, Hodges VC, Hirschfeld DA, Rodriguez MA, McDonald JP, Kotula PG (2013) Nanosecond Pulsed Laser Irradiation of Stainless Steel 304L: Oxide Growth and Effects on Underlying Metal. *Surface and Coatings Technology* 222:1–8.
- [8] Arakha M, Pal S, Samantarrai D, Panigrahi TK, Mallick BC, Pramanik K, Mallick B, Jha S (2015) Antimicrobial Activity of Iron Oxide Nanoparticle Upon Modulation of Nanoparticle-Bacteria Interface. *Scientific Reports* 5:14813.
- [9] Wu S, Altenried S, Zogg A, Zuber F, Maniura-Weber K, Ren Q (2018) Role of the Surface Nanoscale Roughness of Stainless Steel on Bacterial Adhesion and Microcolony Formation. *ACS Omega* 3:6456–6464.
- [10] Zhang X, Wang L, Levänen E (2013) Superhydrophobic Surfaces for the Reduction of Bacterial Adhesion. *RSC Advances* 3(30):12003–12020.
- [11] Gupta RK, Anandkumar B, Choubey A, George RP, Ganesh P, Upadhyaya BN, Philip J, Bindra KS, Kaul R (2019) Antibacterial and Corrosion Studies on Nanosecond Pulse Laser Textured 304L Stainless Steel Surfaces. *Lasers in Manufacturing and Materials Processing* 6(3):332–343.
- [12] Hoek EM, Agarwal GK (2006) Extended DLVO Interactions Between Spherical Particles and Rough Surfaces. *Journal of Colloid and Interface Science* 298(1):50–58.
- [13] Carlson JJ, Kawatra SK (2013) Factors Affecting Zeta Potential of Iron Oxides. *Mineral Processing and Extractive Metallurgy Review* 34(5):269–303.
- [14] Lefèvre G, Cerović L, Milonjić S, Fédoroff M, Finne J, Jaubertie A (2009) Determination of Isoelectric Points of Metals and Metallic Alloys by Adhesion of Latex Particles. *Journal of Colloid and Interface Science* 337(2):449–455.
- [15] Poortinga AT, Bos R, Norde W, Busscher HJ (2002) Electric Double Layer Interactions in Bacterial Adhesion to Surfaces. *Surface Science Reports* 47(1):1–32.
- [16] Carvalho L, Paquentin W, Tabarant M, Maskrot H, Semerok A (2017) Growth of Micrometric Oxide Layer for the Study of Metallic Surfaces Decontamination by Laser. *Proceeding of EPJ Web of Conferences* 153:07038.